Breath visualization: Colorimetric detection of acetone gas using ion-pairing dyes based on hollow silica particles

Jae Jung Park [a,b,1], Jihyun Lee [a,1], Gye Hyeon Kim [a], Jung-Hyun Kim [a], Hyun-Sook Lee [a,*], Wooyoung Lee [a,*]

[a] Department of Materials Science and Engineering, Yonsei University, Seoul 03722, Republic of Korea
[b] KIURI Institute, Yonsei University, 50 Yonsei-ro, Seoul 03722, Republic of Korea

ARTICLE INFO

ABSTRACT

The detection of over 200 volatile organic compounds in exhaled breath has highlighted their potential in diagnosing diseases and monitoring health. Particularly, acetone has emerged as a key biomarker for monitoring ketosis in both healthy individuals and those diagnosed with diabetes. Although equipment-based gas sensor systems such as high-performance liquid chromatography are commonly used for acetone gas detection, they are expensive and require preprocessing. To address these challenges, we developed a cost-effective colorimetric sensor that uses silica-based hollow nanoparticles (SHNPs) and offers enhanced selectivity. We fabricated spherical and uniformly sized SHNPs and infused them with methyl red and brilliant green (M–B ion-pairing dye) to develop colorimetric sensors for acetone gas detection. The optimal color change response occurred at a particle size of 52 ($\pm$ 3.4) nm and shell thickness of 7 ($\pm$ 1.1) nm within the SHNPs, indicative of a significant increase in surface area. Furthermore, the use of hollow silica with a water barrier effect protected the dye, enabling acetone gas detection even in environments with 80% relative humidity. Notably, a substantial color change (Δ130) was noticeable in only 1 min. This robust sensor enables sensitive and rapid naked-eye detection of low concentrations of acetone gas (1 ppm). Consequently, the proposed methodology holds promise for real-time visualization of acetone gas and can be easily integrated into other colorimetric gas sensor systems to enhance both sensitivity and simplicity.

1. Introduction

The identification of over 200 volatile organic compounds in human breath has highlighted the potential of these compounds in applications related to disease diagnosis and health monitoring [1–4]. Among these compounds, acetone has emerged as a valuable biomarker for tracking ketosis in both healthy individuals and those diagnosed with diabetes [1, 2,5]. The detection of minor variations in breath acetone (BrAce) at low ppm levels provides insights into daily activities, satiety, and exercise efficiency [5–11]. Thus, accurate detection of BrAce at low concentrations has the potential to facilitate dietary management, exercise routine development, and disease prevention [2,4,12–14].

Current research in various fields, including clinical analysis, environmental monitoring, biotechnology, pharmaceuticals, and the food industry, is focused on developing acetone gas sensor systems that can effectively monitor trace levels of acetone [7,15–18]. Existing detection systems for acetone gas heavily rely on techniques such as high-performance liquid chromatography (HPLC) [19,20], ion chromatography (IC) [1,21,22], voltammetry [8], amperometry [23], and the use of enzyme electrodes [24] and solid-state sensors [25]. However, these equipment-based systems, including HPLC and IC, often involve pre-treatment procedures and expensive instruments, posing challenges for real-time acetone gas detection [21,26]. To address these limitations, researchers have proposed the use of colorimetric pH sensors based on solid matrices, such as polymer and sol–gel materials, and nanostructured particles [27–29].

Solid matrices are known for their selectivity and other advantageous features, such as permeability, flexibility, and mechanical and

Fig. 1. (a) Schematics of the synthesis of hollow silica particles using phenyltrimethoxysilane (PTMS); Transmission electron microscopy (TEM) images of (b) silica nanoparticles and (c) hollow silica nanoparticles before and after the etching treatment, respectively; (d) Schematics of the acetone gas detection procedure. The exposure of hollow silica particles to acetone gas results in a distinctive color transition from gray to purple, easily detectable by the naked eye.

chemical stability [27–30]. Immobilizing pH indicators in solid matrices can be achieved by applying various methods, including covalent bonding, entrapment, and adsorption [20,23]. Further, the utilization of nanostructured particles, including organic, inorganic, and hybrid materials, has been suggested to augment the capabilities of colorimetric pH sensors, owing to their remarkable attributes such as high sensitivity, extensive surfaces, significant volume ratios, and substantial specific surface areas [31–33]. However, maintaining sensitivity can be challenging due to the potential migration of pH dyes and their susceptibility to moisture, even with fixation methods in place, imposing limitations on the widespread application of pH dyes [33,34]. Recent advancements in color change sensors for acetone have demonstrated the potential use of thymol blue, a pH dye, to produce a visible color change by the specific reaction between acetone and hydroxylamine sulfate [2] Similarly, TCDA (diacetylene monomer 10, 12-tricosadiynoic acid)/-clay/imidazole was employed to achieve a ΔE value of 64.0, indicating a visible color change in acetone gas at 1600 ppm [35]. A polydiacetylene (PDA) incorporated into an aerogel matrix demonstrated heightened sensitivity to acetone relative to various volatile organic compounds (VOCs) and manifested a color change with a ΔE value of 70 at 1000 ppm of acetone [36]. A PCDA (polydiacetylene)-based acetone color sensor with a ΔE value of 92.2 was proposed to produce a color change at 300 ppm of acetone [37]. However, despite these achievements, the application of nanostructured particles in these sensors faces significant challenges, including the difficulty of visual confirmation at low concentrations and vulnerability to humidity. To overcome these challenges, the integration of a hollow silica nanoparticle with an optical pH indicator mechanism affords an efficient colorimetric sensor for visualizing acetone gas [38,39]. The optical pH sensor mechanism induces color changes via the formation of acids or bases resulting from pH variations [40–42].

In this study, we employ hydroxylamine sulfate to produce sulfuric acid in the presence of acetone gas. Using ion pairing, we aim to produce humidity-resistant hydrophobic dyes. We then encapsulate these dyes within hollow silica structures. Subsequently, we synthesize a humidity-resistant M–B dye via ion pairing with a pH dye that is used to coat the nanoparticles. Finally, we analyze the fabricated sensor to assess its response to acetone exposure. This includes determining the detection limit and investigating the effects of concentration, humidity, and exposure time on color changes. This paper introduces a hollow silica-based ion-pairing acetone gas sensor that excels in visually detecting acetone gas, establishing a foundation for future color-changing sensors. The subsequent sections of this paper are structured as follows: Section 2 outlines the materials and methods, Section 3 delves into the results and discussions, and Section 4 concludes the study.

2. Materials and methods

2.1. Materials

We obtained phenyltrimethoxysilane (PTMS, 97%) from Alfa Aesar, while the ammonium hydroxide solution (30 wt% as NH_3) and nitric acid (60%) were sourced from Daejung Chemicals. Daejung Chemicals also provided methanol (99%) and ethanol (99%), which were used as co-solvents and etching reagents. Deionized (DI) water was employed as the main solvent throughout the entire synthesis procedure. All pH dyes, including brilliant green and methyl red, were procured from Sigma Aldrich (MO, USA) and used as received.

2.2. Fabrication of hollow silica particles

Hollow silica nanoparticles were generated through the etching
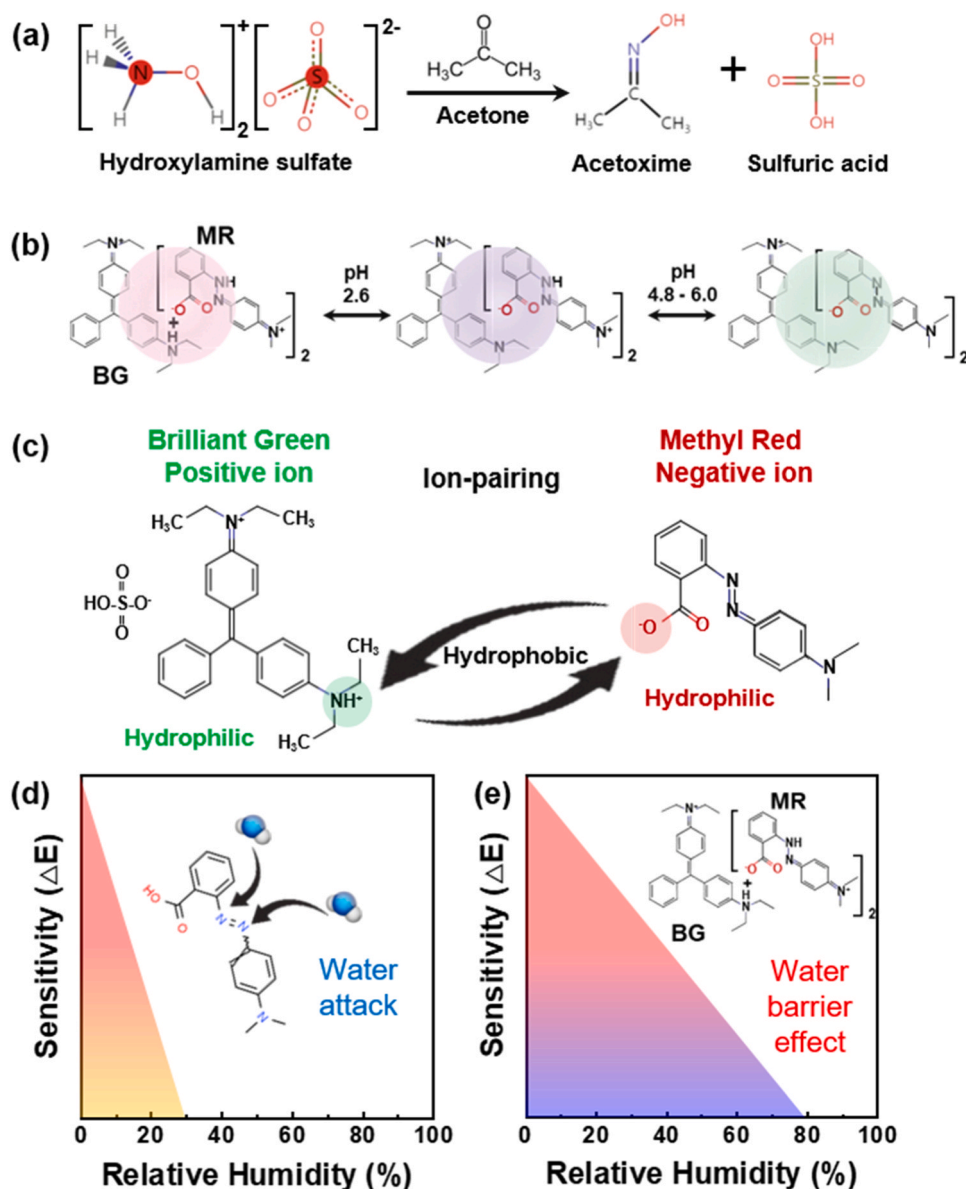
Fig. 2. (a) Acetone sensing mechanism of a dye-based colorimetric sensor that changes color by producing sulfuric acid through the reaction between hydroxylamine sulfate and acetone; (b) Color change of the MR-BG ion-paired dye with the generation of more acid as acetone concentration increases; (c) Ion-pairing mechanism of brilliant green (BG) and methyl red (MR) dye; (d) Reduced sensitivity of pH dyes due to the attack of water molecules; (e) Maintained sensitivity of ion-pairing dyes due to the water barrier effect by possessing relatively hydrophobic sites against water molecules.

process of condensed silica nanoparticles prepared using PTMS [43]. In a 500 mL reactor, DI water (220 mL) was added and stirred while adjusting the internal temperature to 60 ℃. Once the temperature stabilized, HNO₃ (0.14 g) and 0.1–0.5% of PTMS were sequentially added. After 60 s, ammonia and methanol were added in a volume ratio of 7% each, after which the mixture was stirred. The reaction was conducted at 270 rpm for 2 h. Subsequently, Na₂CO₃ (11.86 g) was added as a coagulant to the mixture and stirred for 30 min. The reactor was removed and subjected to three cycles of centrifugation at 1000 rpm for 10 min each. For solvent washing, methanol was used for the first cycle and ethanol was used for the second and third cycles. Etching was performed by sonication at 60 ℃ for 60 min, which yielded the final hollow silica.

2.3. Preparation of a colorimetric sensor for acetone gas detection

To prepare dyes for acetone gas detection, pH dyes brilliant green and methyl red were separately dissolved in a 3:2 solvent mixture of methanol and water, with a volume ratio of 3% each. The solutions were heated (30 ℃) to dissolve the dyes completely. Subsequently, each dye solution was stirred using a mechanical stirrer at 250 rpm for 12 h. After stirring, the precipitated ion-pairing dyes were obtained by filtering the solutions through filter paper to obtain the solid components. The obtained dyes were dried, after which they were dissolved in a 3:2 solvent mixture of methanol and water, containing 3% hydroxylamine sulfate. The resulting solid components were dissolved in methanol at a concentration of 0.15% of the total volume and added to the previous solution. Glycerol was added at a concentration of 5% of the total volume, and the mixture was stirred for approximately 2 h to manufacture the dyes. Thereafter, the ion-pairing dye was coated onto the hollow silica nanoparticles. The dye solution was prepared by dissolving the dye (0.4 g) in ethanol (20 mL). Subsequently, the dye solution (0.4 μL) was added to a hollow silica nanoparticle dispersion (5 mL), and the mixture was stirred for 3 h to obtain an acetone gas detection sensor. During this
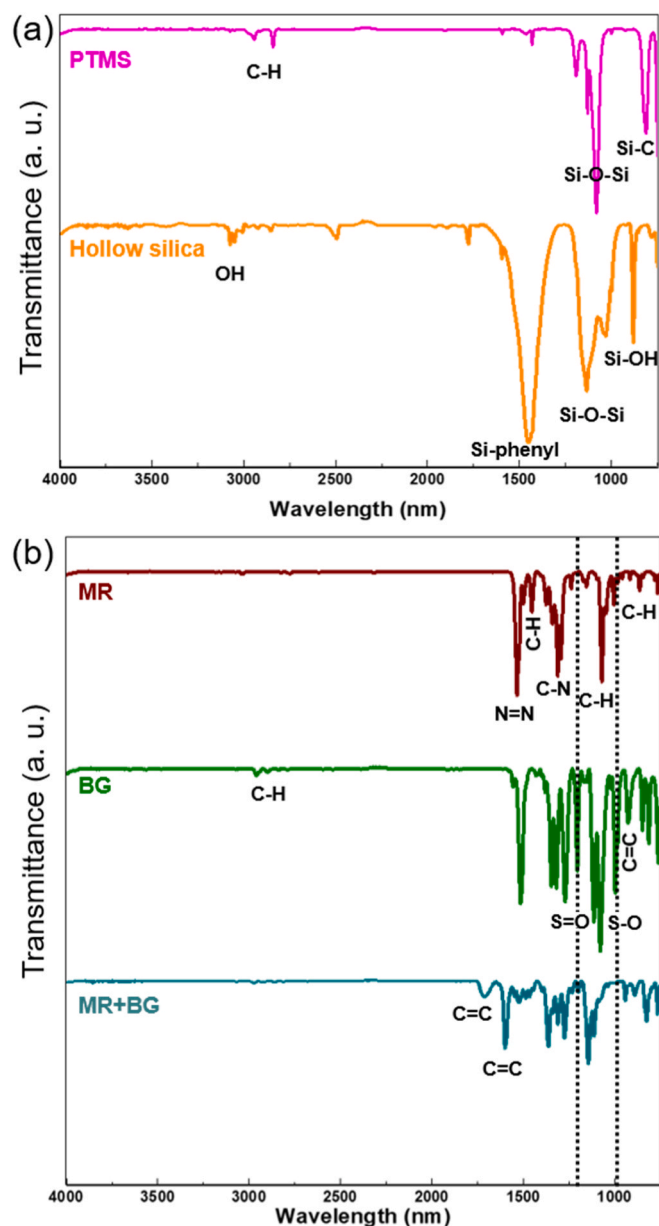
Fig. 3. The FT-IR spectra: (a) PTMS and hollow silica; (b) methyl red (MR), brilliant green (BG), and ion paring (MR+BG) dyes.

process, the sensor was washed three times with DI water to remove residual dye, filtered, and dried in a vacuum oven (30 °C) for 12 h to yield an acetone gas sensor powder. Subsequently, the powder was dispersed in an acrylic binder and coated onto a polyethylene tere-phthalate (PET) film.

2.4. Evaluation of the sensing performance of the colorimetric sensor

The performance of the hollow silica-based gas sensors was evaluated in a tube furnace system equipped with mass flow controllers (MFCs). The furnace temperature and gas flow rate were automatically controlled using customized LabView software. Acetone gas was generated using standard gases obtained from a company. The gas concentration was adjusted by controlling the gas flow rate of the MFCs, using dry synthetic air as the balancing gas. The target gas and synthetic air as the carrier gas at specific concentrations were introduced into the chamber at a constant flow rate of 1000 sccm. The performance of the sensor in detecting acetone gas with various dyes was investigated by exposing them to different gas concentrations and humidities (0–80%) for 0–10 min. The color change images of the sensor were captured using a digital scanner (HP Scanjet pro 3500) before and after exposure to acetone. In each image, the RGB values were extracted using the Photoshop program. Average RGB values were obtained on several spots in each sensor. The colorimetric response was assessed using the Euclidean distance formula (ΔE), calculated as $\Delta E = (\Delta R^2 + \Delta G^2 + \Delta B^2)^{1/2}$, representing the difference of the R, G, and B values before and after exposure. A representative ΔE value for each acetone concentration was determined by averaging the values from five sensors. The sensing tests were performed on approximately 88 sensors, and they exhibited a similar trend for the same acetone concentration.

2.5. Morphological analysis of hollow silica nanoparticles

The prepared hollow silica nanoparticles were subjected to morphological analysis using scanning electron microscopy (JEOL JSM6700, Japan). Drops of the prepared emulsion nanoparticles were deposited onto a silicon wafer and dried at 25 °C for 10 h. The hollow structure of the nanoparticles was observed using transmission electron microscopy (TEM, JEM-F200, Japan). For sample preparation, one or two drops of single nanoparticles and the hollow silica nanoparticles dispersed in DI water were placed on carbon-coated copper grids and dried at 25 °C for 12 h. The atomic distribution of elements in the nanostructure of the acetone-gas-responsive detector was evaluated by energy-dispersive X-ray spectroscopy. The particle size distribution of the synthesized nanoparticles was analyzed using a Zetasizer nano system (Zetasizer nano ZS90, UK). The diluted sample was further diluted to approximately 1 wt% using DI water before analysis.

3. Results and discussion

In this study, we developed a hollow silica-particle-based acetone detector that exhibits visible color changes upon reacting with dyes in the presence of acetone gas. Fig. 1(a) schematically describes the manufacturing process of hollow silica particles. Phenyl-trimethoxysilane (PTMS) monomers are dissolved in deionized water at temperatures ranging from 30 to 70 °C and react at a temperature surpassing the phase transition temperature of the monomer. This process is conducted with vigorous stirring to ensure homogeneity in the reaction medium. Thereafter, acidification and hydration occur, and an ammonium hydroxide solution is introduced to promote the formation of primary particles through interfacial bonding between liquid droplets. These primary particles then undergo polymerization, establishing a shell structure. The interior of the shell is subsequently etched using ethanol, creating the desired hollow cavity. The final product, namely, a powder consisting of hollow silica particles, is obtained through filtration and drying procedures. Fig. 1(b) and (c) display transmission electron microscopy (TEM) images that illustrate the formation of hollow particles through etching after the production of individual particles. Notably, the TEM image in Fig. 1(c) illustrates the transformation of the particle structure into a distinct core-shell configuration, indicative of a significantly enlarged specific surface area. Subsequently, ion-pairing dyes are applied to coat the hollow silica particles and assemble the acetone gas-responsive detector (Fig. 1(d)).

Fig. 2 illustrates the sensing mechanism of the colorimetric acetone sensor and ion-pairing mechanism of brilliant green (BG) and methyl red (MR) dyes. The interaction between acetone gas and the hydroxylamine sulfate molecules, used as solvent in the dye, leads to observable color changes in the ion-pairing dyes incorporated into the carrier containing hollow silica particles. As shown in Fig. 2(a), this interaction occurs via the formation of acetoxime and sulfuric acid by the reaction between hydroxylamine sulfate and acetone gas, resulting in pH variations that trigger visible color changes in the ion-pairing dyes within the hollow silica particles. Based on this process, when the M–B ion-pairing dye was exposed to a certain concentration of acetone, the color changes from
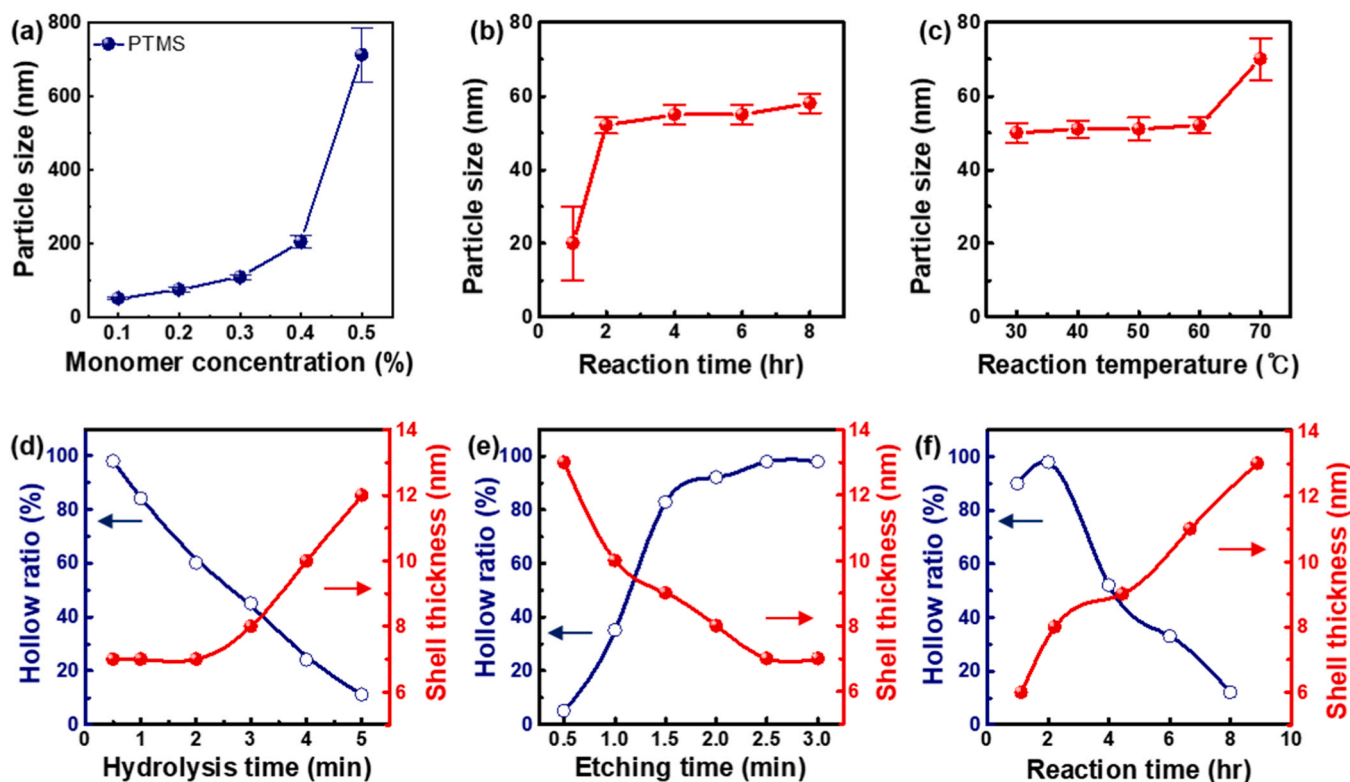
Fig. 4. Particle size and porosity control: Examining the impacts of (a) monomer concentration, (b) reaction time, and (c) reaction temperature on particle sizes. Assessing the variation in hollow ratio and shell thickness of hollow silica nanoparticles at different fabrication times for (d) hydrolysis, (e) etching, and (f) reaction.

dark green to purple. Subsequently, with further gas reaction, it finally shifts to a faint pink color (Fig. 2(b)). During this process, the chemical state of the sensor undergoes a change, leading to a persistent color alteration. Therefore, the color of the M–B ion-pairing dye sensor does not revert to its original color after the removal of acetone gas. Similarly, colorimetric acetone sensors based on pH dyes [2,44], operating on the same sensing mechanism, also exhibit irreversibility.

Fig. 2(c) depicts the process of synthesizing a new dye through ion pairing, involving BG and MR dyes with positive and negative ions, respectively. Positive N^+ ions, bonded with the methyl group (CH_3) in the BG dye, and negative OH^- ions, bonded with the carboxyl (COOH) group in the MR dye, are paired. The typical pH dye like MR or BG becomes vulnerable to water molecule attacks, leading to reduced sensitivity in high-humidity conditions (Fig. 2(d)). However, Fig. 2(e) demonstrates that the M–B ion-pairing dye possesses relatively hydrophobic sites, creating a water barrier effect that maintains sensitivity even when subjected to water molecule attacks in high-humidity conditions.

Fourier-transform infrared (FT-IR) spectroscopy was conducted to determine the chemical bonding of the synthesized hollow silica, and the results are shown in Fig. 3(a). The FT-IR spectra of the hollow silica nanoparticles showed absorption peaks at 1030 and 1130 cm^{-1}, which are attributed to the Si-O-Si stretching bands within the silica framework. In addition, the appearance of a peak at 1450 cm^{-1} was attributed to the presence of the Si-phenyl group, confirming the attachment of the phenyl group to the surface of hollow silica nanoparticles. In the chemically etched particles, absorption peaks were predominantly observed at approximately 3300–3500 cm^{-1}, arising from adsorbed water and Si-OH hydroxyl groups. However, weak absorption peaks from the phenyl groups could still be identified, indicating that the aromatic desilylation reaction was not fully completed under the experimental conditions. Conversely, in the thermally treated particles, the absorption peak related to the Si-O-Si stretching bond was the sole peak observed, indicating a complete conversion to pure inorganic silica

particles. Furthermore, FT-IR analysis was conducted to investigate the chemical bonding of the M–B ion-pairing dye (Fig. 3(b)). In the case of brilliant green (BG) bonded with hydrogen sulfate (HSO_4^-), distinct absorption bands of S=O and S-O appear at 1203 and 999 cm^{-1}, respectively. Interestingly, these characteristic bands are absent in the IR spectrum of the M–B ion-pairing dye, indicating the replacement of hydrogen sulfate with a different anionic ion, potentially originating from an anionic dye. Additionally, new peaks at ~1600 and ~1700 cm^{-1}, arising from the C=C bands belonging to the aromatic ring of MR and BG, were observed for the M–B ion-paired dye. In the IR spectrum of the M–B ion-paired dye, the disappearance of S=O and S-O peaks, along with the appearance of C=C peaks, may indicate that the M+B dye becomes hydrophobic through ion-pairing. FT-IR analysis suggested that intermolecular Coulomb forces drive the attraction between oppositely charged dyes, causing them to associate as one molecule.

Hollow silica nanoparticles were fabricated to encapsulate dyes under various condition, as shown in Fig. 4. To maximize the specific surface area before the fabrication of hollow silica nanoparticles, the sizes of small silica nanoparticles were controlled. Fig. 4(a) presents a graph depicting the variation in particle size with changes in monomer concentration. PTMS at different concentrations (0.1%, 0.2%, 0.3%, 0.4%, and 0.5%) was used to determine the effect of monomer concentration on particle size. The results demonstrated a gradual increase in particle size with an increase in monomer concentration, with average particle sizes of 52, 76, 109, 206, and 712 nm at concentrations of 0.1%, 0.2%, 0.3%, 0.4%, and 0.5%, respectively. Furthermore, at a monomer concentration of 0.5%, a significant increase in particle size was observed, along with a non-uniform particle distribution. This can be attributed to the increased number of hydrolyzed monomers that can influence the particle size, leading to accelerated particle growth during condensation. Therefore, for the experiments, the monomer concentration was adjusted to 0.1% based on these observations. Fig. 4(b) illustrates the variation in particle size with respect to changes in reaction
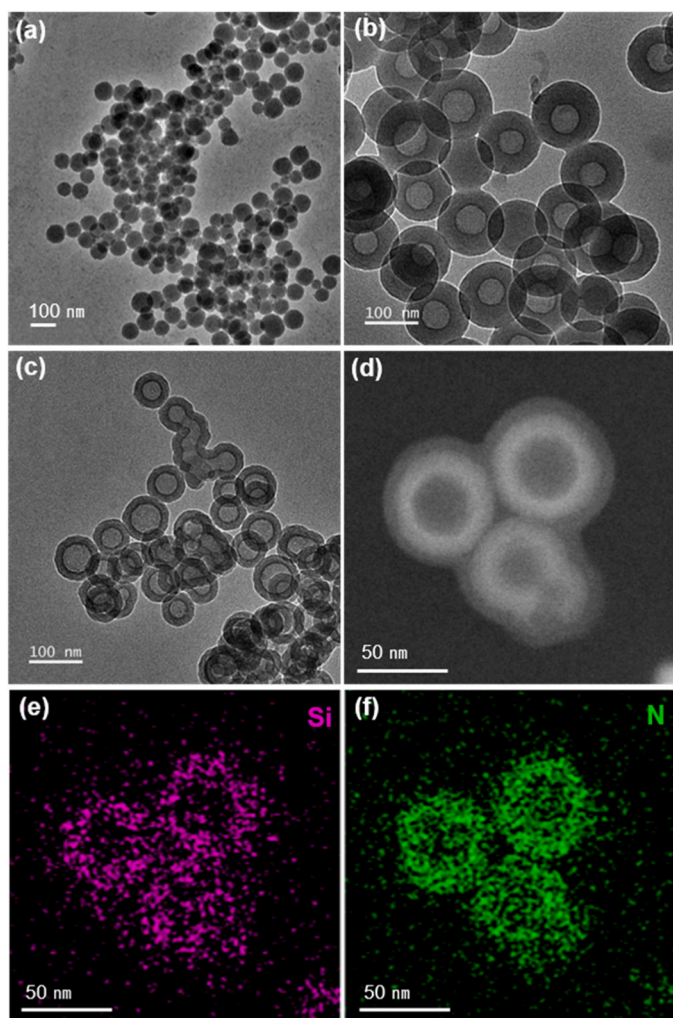
Fig. 5. TEM images: (a) condensed silica particles, hollow silica particles (b) before and (c) after adjusting hollow ratio and shell thickness, and (d) magnified view of the optimized hollow silica particles. EDS images to confirm the presence of dye encapsulation within hollow silica particles: (e) Si mapping image showing distribution of Si within the hollow silica and (f) N mapping image showing the distribution of N, originating from the dye, both on the surface and in the internal structure of hollow silica particles.

time. By varying the reaction time to 1, 2, 4, 6, and 8 h, changes in the particle size were observed. After 1 h, the results indicated an average particle size of 20 nm but with a non-uniform distribution. From 2 h onwards, the particle sizes remained constant at 52, 55, 56, and 58 nm after 2, 4, 6, and 8 h, respectively, with a uniform particle distribution. This suggests that, after a reaction time of 2 h, the particle size stabilizes. Fig. 4(c) presents a graph demonstrating the effect of reaction temperature on particle size. By increasing the reaction temperature from 30 to 70 °C, changes in particle sizes were observed. Based on these results, a monomer concentration of 0.1%, reaction time of 2 h, and temperature of 30 °C were selected as the optimal conditions. Under these optimal conditions, the optimum particle size was determined to be approximately 50 nm.

Fig. 4(d) depicts a graph showing the variation in the hollow ratio and shell thickness based on hydrolysis time control. The hydrolysis time was adjusted to 0.5, 1, 2, 3, 4, and 5 min. The results showed a decrease in the hollow ratio from 98%, 84%, 60%, 45%, 24%, to 11% as the hydrolysis time increased and an increase in the shell thickness of the hollow particles to 7 ($\pm$ 1.1), 7 ($\pm$ 1.3), 7 ($\pm$ 1.5), 8 ($\pm$ 2.1), 10 ($\pm$ 2.2), and 12 ($\pm$ 3.5) nm, respectively. These findings indicate that the hydrolysis time influences the hollow ratio and shell thickness. The

observed phenomenon can be attributed to the extended coalescence reaction time of particles, which results in a more robust core that is resistant to etching, leading to a decrease in the hollow particle ratio and an increase in the shell thickness. Based on these reasons, the hydrolysis time was set to 0.5 min for the fabrication of hollow silica.

Fig. 4(e) illustrates the variation in the hollow ratio and shell thickness with different etching times. Following etching periods of 0.5, 1, 1.5, 2, 2.5, and 3 min, the hollow ratio showed a steady increase after reaching 92%, eventually stabilizing at 98% (5%, 35%, 83%, 92%, 98%, to 98%, respectively), while the shell thickness of the hollow particles decreased to 13 ($\pm$ 3.8), 10 ($\pm$ 2.4), 9 ($\pm$ 2.2), 8 ($\pm$ 1.8), 7 ($\pm$ 1.4), and 7 ($\pm$ 1.1) nm, respectively. After 2 min, the shell thickness remained constant. This observation suggests that an insufficient etching time led to these outcomes. Therefore, in this study, an etching time of 2 min was chosen to maintain an adequate hollow ratio.

Fig. 4(f) presents the variation in the hollow ratio and shell thickness with different reaction times. After reaction times of 1, 2, 4, 6, and 8 h, the hollow ratios were 90%, 98%, 52%, 33%, and 12%, respectively, as single particles transformed into hollow particles, and the corresponding shell thicknesses of the hollow particles were 6 ($\pm$ 4), 8 ($\pm$ 2), 9 ($\pm$ 1), 11 ($\pm$ 1), and 13 ($\pm$ 6) nm, respectively. These trends differed from those observed under the previously studied condition variations. Specifically, the hollow ratio remained similar between 1 and 2 h, while the shell thickness decreased initially before increasing. This suggests that, during the initial 1 h of the reaction, an inadequate reaction time often resulted in particle deformation during etching. However, after 2 h, a sufficient reaction time led to a higher hollow ratio and shell thickness. After 3 h of the reaction, a prolonged reaction time made the core stronger, leading to a reduced hollow ratio and a thicker shell in the resulting hollow silica particles. Consequently, by utilizing the optimal silica particle size of approximately 50 nm and employing the optimal conditions for hollow fabrication—0.5 min of hydrolysis time, 2 min of etching time, and 2 h of reaction time—we were able to produce hollow silica nanoparticles with a maximum hollow ratio and a shell thickness of approximately 7 nm. This optimal size of hollow silica nanoparticles led to the most favorable acetone response.

Fig. 5(a) shows a TEM image of the original silica nanoparticles used for further preparation of the hollow particles. Fig. 5(b) shows a TEM image of the nanoparticles before adjusting the shell thickness and hollow ratio, which can be influenced by various factors. Fig. 5(c) and (d) demonstrate hollow silica particles with consistent shell thicknesses and hollow ratios prepared under the optimized process conditions. To confirm dye encapsulation within these hollow silica particles, a TEM-EDS analysis was conducted. The results of this analysis indicate that Si, which constitutes the hollow silica, is exclusively observed on the outer wall (Fig. 5(e)), while N, which originates from the dye, is uniformly distributed on both the surface and the internal structure of the particles (Fig. 5(f)). This observation strongly suggests that the hollow silica efficiently encapsulates the dye.

Fig. 6(a) displays actual photos of the M-B ion-pairing dye sensors exhibiting color changes before acetone exposure and after the reaction with 10 ppm acetone over exposure times ranging from 1 to 10 min Fig. 6(b) and (c) display the color change images of methyl red (MR) dye, a conventional pH dye, and M–B ion-paired dyes in response to various acetone concentrations (1, 5, and 10 ppm) over different exposure times (0–10 min), respectively. Notably, the brilliant green dye (BR) sensor did not exhibit color change under the same conditions. Consequently, our comparison focused on MR and M-B ion-pairing dyes. The results were obtained at a temperature of 25 °C and humidity of 10%RH. As shown in Fig. 6(b), using methyl red, color changes were observed at 1, 5, and 10 ppm, but they were manifested as subtle variations in similar shades, making visual determination challenging. In contrast, Fig. 6(c) demonstrates a distinct color change from grayish-green to purple for the M–B ion-pairing dye as the acetone concentration was increased from 1 through 5 to 10 ppm. In particular, a clear color change was observed even at 1 ppm acetone with a short exposure
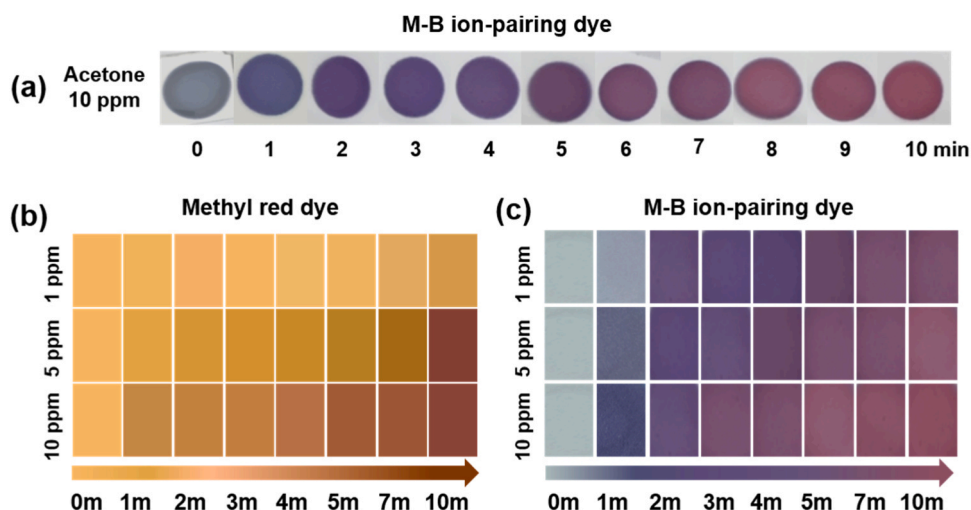
Fig. 6. (a) Photos of the M–B ion-paired dye sensor after the reaction with 10 ppm acetone for various exposure times, ranging from 0 to 10 min. Color change images of (b) methyl red dye, a typical pH dye and (c) M–B ion-paired dyes in response to different acetone concentrations (1, 5, and 10 ppm) for various exposure times (0–10 min). The color change measurements were conducted at 25 ℃ and 10% RH conditions.
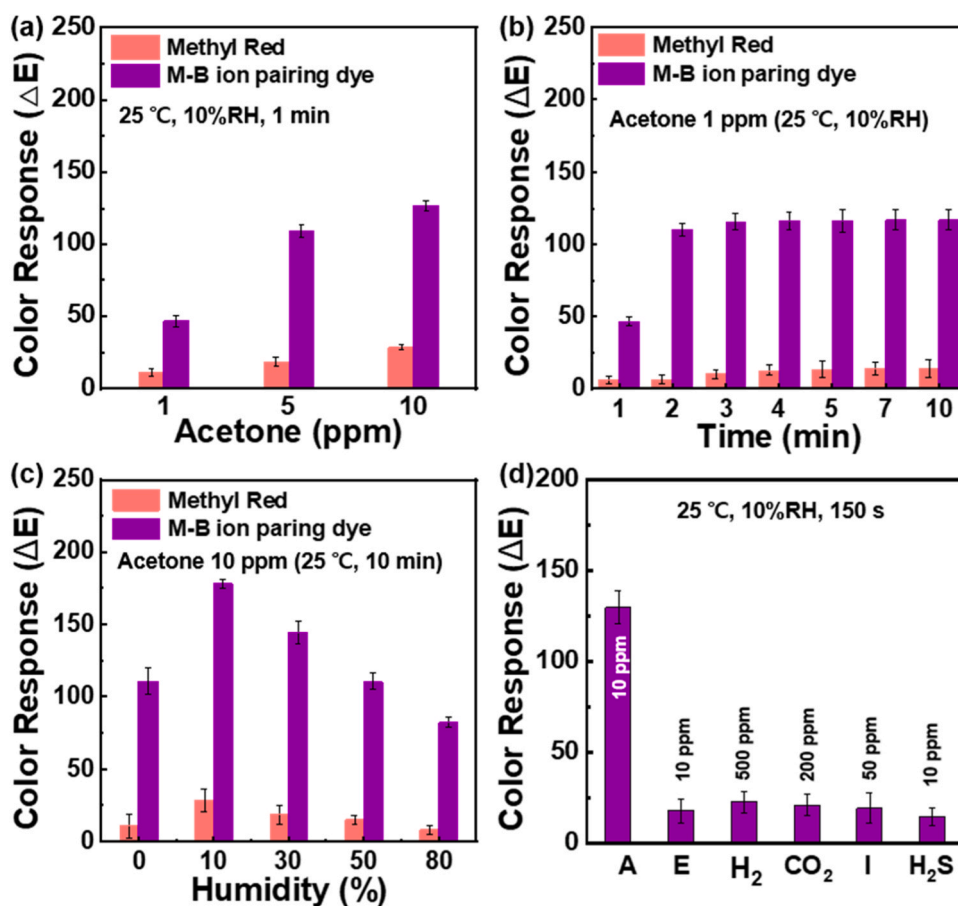

Fig. 7. (a)-(c) Comparison of Colorimetric response (ΔE) in methyl red and M-B ion-pairing dyes under various measurement conditions: (a) different acetone concentrations of 1, 5, and 10 ppm for 1 min of exposure, (b) 1 ppm acetone for different exposure times (1–10 min), (c) 10 min exposure of 10 ppm acetone under different humidity conditions (0–80%). (d) Colorimetric response of M-B ion-pairing dye to various test gases (acetone(A) 10 ppm, ethanol(E) 10 ppm, H_2 500 ppm, CO_2 200 ppm, isoprene 50 ppm, and H_2S 10 ppm) for 150 s exposure at 25 ℃ and 10% RH conditions.

time of 1 min. The results highlighted the high sensitivity of the M–B ion-pairing dye to even slight pH variations.

Fig. 7(a) graphically illustrates the variations in the colorimetric response (ΔE) values at different concentrations of acetone gas (1, 5, and

10 ppm). In all cases, acetone exposure was conducted for 1 min at a temperature of 25 ℃ and humidity of 10%. At acetone gas concentrations of 1, 5, and 10 ppm, respectively, the methyl-red-based acetone sensor showed ΔE values of 11.0, 18.5, and 28.5, while the M–B ion-
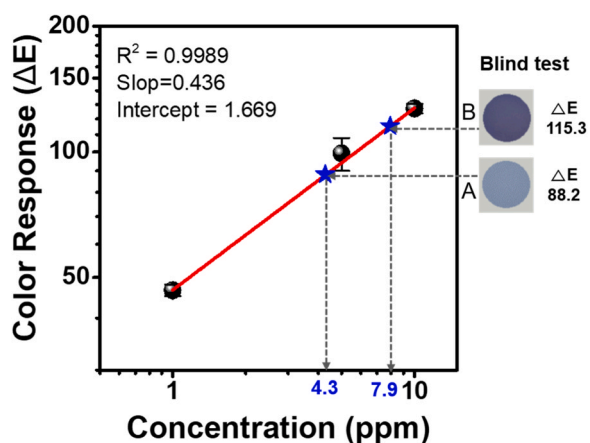
Fig. 8. Blind test results for M–B ion-paired dye sensors "A" and "B," exposed to two unknown concentrations of mixed acetone by a third party. The unknown acetone concentrations of the blind-tested sensors were determined using a calibration curve established in a log-log scale plot.

pairing dye exhibited ΔE values of 46.6, 108.8, and 127.0. Both dyes exhibited an increase in ΔE with increasing concentration of acetone gas. However, for the methyl red-based sensor, at all studied acetone concentrations, ΔE values were below 30, and clear visual change was not observed. In contrast, the M–B ion-pairing dye showed ΔE values exceeding 30 at all studied concentrations of acetone and noticeable visual changes. Even at the lowest concentration of 1 ppm, its ΔE was measured to be 46.6. The results indicate that the M–B ion-pairing dye displays higher sensitivity and enables a noticeably clearer visual identification than methyl red. This heightened sensitivity is attributed to the pH changes resulting from the generation of minute quantities of sulfuric acid.

Fig. 7(b) graphically illustrates the change in ΔE over time when exposed to 1 ppm acetone gas for 10 min. The results show that the methyl-red-based acetone sensor produced ΔE values of 5.8, 6.4, 10.2, 12.5, 13.6, 13.8, and 14, while the M–B ion-pairing dye-based one yielded ΔE values of 46.6, 110.2, 115.6, 116.1, 116.2, 116.5, and 116.8, after 1, 2, 3, 4, 5, 7, and 10 min, respectively. The ΔE values of the methyl-red-based acetone sensor were all under 15 and it did not exhibit a noticeable color change even after 10 min of exposure to 1 ppm acetone. In addition, the ΔE values showed minimal variation after 3 min. In contrast, the M–B ion-pairing dye-based acetone sensor displayed a noticeable color change when ΔE exceeded 40 after 1 min of exposure. A rapid increase in ΔE values was observed up to 2 min, after which the rate of increase reached saturation. These findings suggest that the initial 1-min exposure to acetone gas caused pH alterations, resulting in a relatively consistent response during prolonged exposure.

In conclusion, the M–B ion-pairing dye-based acetone gas sensor demonstrates swift color changes irrespective of the acetone concentration, with the ΔE value peaking at 116.8. Therefore, it enables the immediate detection of minute traces of acetone gas present in human breath.

Fig. 7(c) displays a graph showing the variations in ΔE when 10 ppm acetone gas is exposed to different humidity levels (10%, 20%, 30%, 50%, and 80%) at a temperature of 25 °C for 10 min. The results indicate that the methyl-red-based acetone sensor yielded ΔE values of 10.7, 28.5, 18.68, 15.25, and 8.13, while the M–B ion-pairing dye-based sensor produced ΔE values of 110.7, 178.2, 94.45, 72.54, and 52.31, respectively. These findings suggest that the methyl-red-based sensor has a lower resistance to humidity than that using the M–B ion-pairing dye. Moreover, when the humidity exceeded 50%, the ΔE values of the methyl-red-based sensor decreased by 47% compared with the ΔE values at 10% humidity. In contrast, the M–B ion-pairing dye-based sensor exhibited a ΔE value of 52.31 even at humidity levels exceeding 80%, making it visually detectable. In addition, at humidity levels above 50%, its ΔE decreased by 38% compared with that at 10% humidity, indicating a 9% improvement in humidity resistance for the M–B ion-pairing dye-based acetone sensor compared with the methyl-red-based one at the same humidity. This improvement can be attributed to the water barrier effect of the M–B ion-pairing dye. Unlike the commonly used methyl red dye, which is susceptible to sensitivity reduction owing to reaction with water molecule, the M–B ion-pairing dye exhibits relatively more hydrophobic properties owing to ion pairing, affording reduced susceptibility to humidity. Furthermore, the sensitivity increases as humidity increased from 0% to 10% and then decreased at humidity above 10%. This color change stems from humidity conditions, under which imine formation increases the positive charge during nucleophilic addition reactions.

Fig. 7(d) displays the colorimetric response (ΔE) graph for various gases found in human exhaled breath. These color changes were observed after 150 s of exposure at a temperature of 25 °C and humidity of 10%. For acetone (10 ppm), ethanol (10 ppm), H_2 (500 ppm), CO_2 (200 ppm), isoprene (50 ppm), and H_2S (10 ppm), the corresponding ΔE values were measured at 130.1, 17.8, 22.46, 21.1, 19.4, and 14.3, respectively. Notably, the M–B ion-pairing dye exhibited a significantly high ΔE for acetone. In line with a previous report by Sha et al. [44], methyl red dye used in a solution form showed the limit of detection (LOD) for acetone at 0.02 ppm but displayed an equal response to acetone and ethanol. It is essential to highlight that the M–B ion-pairing dye demonstrates clear selectivity towards acetone gas. The findings suggest that the ion-pairing configuration of the M–B dye has a more favorable condition for generating sulfuric acid through the reaction between acetone gas and hydroxylamine sulfate. Moreover, this reaction occurs within a time frame of 150 s, which facilitates facile visual detection of trace amounts of acetone gas.

Additionally, we carried out a validation of sensor performance
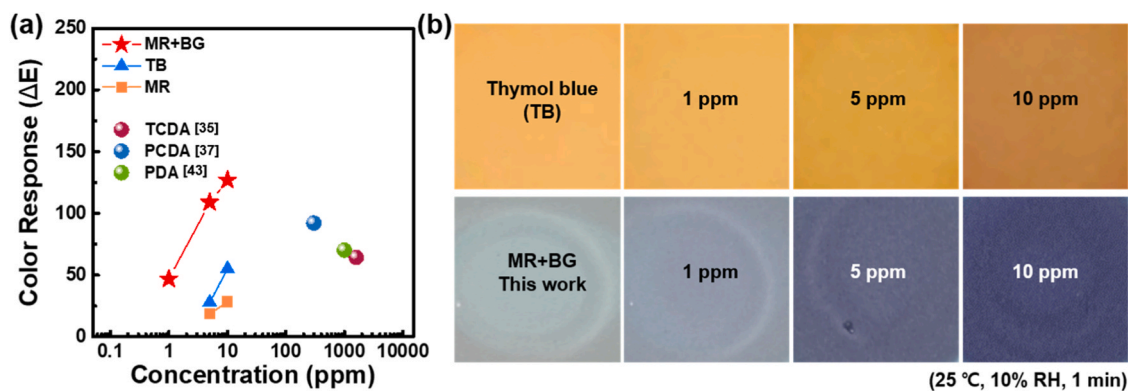
Fig. 9. (a) Comparison of the color change capabilities of the acetone sensor developed in this study with the sensors developed by other groups. (b) Visual changes in acetone gas sensors fabricated using thymol blue (TB) and the one developed in this study.

based on the determination of the unknown concentration of acetone using the M-B ion-paired dye sensors. A blind test was conducted with M–B ion-paired dye sensors "A" and "B", which were exposed to two unknown concentrations of acetone mixed by a third party (Fig. 8). The blind test followed the same conditions as the previous experiments, comprising a 1-minute exposure at 25 °C and 10% RH. The color response values ($\triangle$E) of the sensors from the blind test were determined by calculating RGB values from actual photos. The $\triangle$E values were 88.2 for the "A" sensor and 115.3 for the "B" sensor (Fig. 8). To ascertain the unknown concentrations of the two sensors, we established a calibration curve using the color change images of M–B ion-paired dyes prepared at known acetone concentrations of 1, 5, and 10 ppm, which were extracted from Fig. 6(a). Since the colorimetric response is not linear with concentration, we used a log-log scale plot for the calibration curve. The nonlinear relationship between sensing response and gas concentration could be completely linearized by a log-log transformation (R^2 =0.9989). Consequently, the acetone concentrations of the blind-tested sensors "A" and "B" were determined as 4.3 and 7.9 ppm, respectively, as shown in Fig. 8. These values are reasonable even when compared with the naked eye.

Fig. 9(a) provides an overview of the status of sensors capable of visible color change with the naked eye upon exposure to acetone gas. Notably, Hussain et al.[35] used a TCDA/clay/imidazole system and achieved a $\triangle$E value of 64.0, indicating a visible color change in the presence of 1600 ppm of acetone gas for a 6-minute exposure. Kim et al. [37] proposed a PCDA-based acetone color sensor with a $\triangle$E value of 92.2 when exposed to 300 ppm acetone. In addition, Dolai et al. [36] reported that a PDA-aerogel hybrid composite functioned as a colorimetric acetone sensor, exhibiting a visible color change with a ΔE value of 70 at 1000 ppm of acetone for a 10-minute exposure [36]. Here, the values of ΔE and acetone concentration values of TCDA, PCDA, and PDA sensors were estimated from the actual color change images after acetone reaction presented in the paper.

We additionally evaluated the sensing capability of the sensor incorporating thymol blue (TB) dye encapsulated within the hollow silica nanoparticles under the same conditions of 1-minute acetone exposure at 25 °C and 10% RH. A comparison of the visual color changes of the two sensors is presented in Fig. 9(b). While the acetone sensor using TB only exhibited a concentration-dependent color change at 5 ppm, the sensor developed in this study demonstrated a significantly pronounced variation visible to the naked eye even at 1 ppm. It is important to note that the reported LOD values in other colorimetric sensors, such as TB casted on a silica gel substrate [2] and 2,4-dinitrophenylhydrazine (DNPH)-impregnated porous glass [45], were approximately 0.6 ppm and 0.1 ppm, respectively. However, these values were calculated using absorbance recorded in real-time during color changing, while we utilized the converted ΔRGB values of the color change after the reaction. Additionally, resorcinol-imbibed membranes exhibited a distinct color change at 2 ppm acetone, visible to the naked eye [46]. Accordingly, it is noteworthy that our LOD of 1 ppm for naked-eye detection implies the highly sensitive reaction of M-B ion-pairing dye with acetone gas molecules.

As shown in Fig. 9(a), the pH dye-based sensor constructed on hollow silica nanoparticles demonstrated a visible color change at low concentrations of acetone, surpassing other reported sensors. This indicates that sensors causing pH changes through the generation of sulfuric acid from the reaction of acetone gas with hydroxylamine sulfate are more effective in acetone colorimetric detection. In particular, the M–B ion-pairing dye demonstrated the most sensitive color change compared to other dyes, such as MR and TB. This sensitivity can be attributed to the distinct pH values of each dye, resulting in varying levels of increased acidity (Fig. S1). In the case of MR dye, the color transition occurs from yellow to red as the pH decreases from 6 to 4.3. For TB dye, the color change happens from yellow to red when the pH decreases from 3 to 1. Meanwhile, the M-B ion-pairing dye exhibits a color shift from green-gray to purple and magenta as the pH decreases from 5 to 3.5 and 2,

respectively. At the same concentration of acetone gas, the pH values fall within the range of 5 to 2, as indicated in Fig. S1. As a result, the sequence of color change is extensive in the following order: MR, TB, and M-B ion-pairing dyes. Consequently, the observed trend of differences in acetone sensitivity among the prepared dyes, as depicted in Fig. 8(a), is well understood. Therefore, the newly proposed M-B ion-pair dye has been confirmed to be well-suited for functioning as a highly sensitive colorimetric sensor, capable of detecting low concentrations of acetone, even at the 1 ppm level.

4. Conclusion

In this study, researchers developed a hollow silica particle-based acetone detector that exhibited visible color changes when exposed to acetone gas. This detector utilized a newly synthesized M–B ion-pairing dye, which demonstrated an improved sensitivity and selectivity for acetone compared to the previously reported dyes like methyl red. It showed high sensitivity even at low concentrations of acetone gas, with significant color changes observed within 1 min of exposure. The detector also exhibited excellent humidity resistance and maintained its visual detection capabilities even at high humidity (above 80%). Overall, this detector, which combined hollow silica particles and the M–B ion-pairing dye, demonstrated remarkable sensitivity, selectivity, and humidity resistance, enabling the detection of trace amounts of acetone gas, and has potential applications in healthcare and environmental monitoring.

CRediT authorship contribution statement

Lee Jihyun: Writing – original draft, Validation, Investigation, Data curation. **Park Jae Jung:** Writing – original draft, Validation, Conceptualization. **Lee Wooyoung:** Supervision, Project administration, Funding acquisition. **Kim Jung-Hyun:** Validation, Conceptualization. **Lee Hyun-Sook:** Data curation, Validation, Writing – review & editing. **Kim Gye Hyeon:** Data curation.

Declaration of Competing Interest

The authors declare that they have no known competing financial interests or personal relationships that could have appeared to influence the work reported in this paper.

Data availability

Data will be made available on request.

Appendix A. Supporting information

Supplementary data associated with this article can be found in the online version at doi:10.1016/j.snb.2024.135373.

References

[1] K. Dixit, S. Fardindoost, A. Ravishankara, N. Tasnim, M. Hoorfar, Exhaled breath analysis for diabetes diagnosis and monitoring: relevance, challenges and possibilities, Biosensors 11 (2021) 476, https://doi.org/10.3390/bios11120476.

[2] D. Wang, F. Zhang, A. Prabhakar, X. Qin, E.S. Forzani, N. Tao, Colorimetric sensor for online accurate detection of breath acetone, ACS Sens. 6 (2021) 450–453, https://doi.org/10.1021/acssensors.0c02025.

[3] Q.A. Drmosh, I. Olanrewaju Alade, M. Qamar, S. Akbar, Zinc oxide-based acetone gas sensors for breath analysis: a review, Chem. Asian J. 16 (2021) 1519–1538, https://doi.org/10.1002/asia.202100303.

[4] M.R. Hossain, Q. Zhang, M. Johnson, O. Ama, D. Wang, Investigation of different materials as acetone sensors for application in type-1 diabetes diagnosis, Biomed. J. Sci. Tech. Res. 14 (2019) 10940–10945, https://doi.org/10.26717/BJSTR.2019.14.002619.

[5] Y. Obeidat, The most common methods for breath acetone concentration detection: a review, IEEE Sens. J. 21 (2021) 14540–14558, https://doi.org/10.1109/JSEN.2021.3074610.

[6] M. Šetka, F.A. Bahos, D. Matatagui, I. Gràcia, E. Figueras, J. Drbohlavová, S. Vallejos, Love wave sensors with silver modified polypyrrole nanoparticles for VOCs monitoring, Sensors 20 (2020) 1432, https://doi.org/10.3390/s20051432.

[7] M. Righettoni, A. Tricoli, S.E.S. Pratsinis, Si:WO₃ sensors for highly selective detection of acetone for easy diagnosis of diabetes by breath analysis, Anal. Chem. 82 (2010) 3581–3587, https://doi.org/10.1021/ac902695n.

[8] S.M. Hicks, A.J. Killard, Electrochemical impedance characterisation of tungsten trioxide–polyaniline nanocomposites for room temperature acetone sensing, Sens. Actuators B. 194 (2014) 283–289, https://doi.org/10.1016/j.snb.2013.12.047.

[9] D. Zhang, Z. Wu, X. Zong, Metal-organic frameworks-derived zinc oxide nanopolyhedra/s, N: graphene quantum dots/polyaniline ternary nanohybrid for high-performance acetone sensing, Sens. Actuators B. 288 (2019) 232–242, https://doi.org/10.1016/j.snb.2019.02.093.

[10] G. Liu, L. Zhu, Y. Yu, M. Qiu, H. Gao, D. Chen, WO₃ nanoplates for sensitive and selective detections of both acetone and NH₃ gases at different operating temperatures, J. Alloy. Compd. 858 (2021) 157638, https://doi.org/10.1016/j.jallcom.2020.157638.

[11] Q. Ding, Y. Wang, P. Guo, J. Li, C. Chen, T. Wang, K. Sun, D. He, Cr-doped urchin-like WO₃ hollow spheres: the cooperative modulation of crystal growth and energy-band structure for high-sensitive acetone detection, Sensors 20 (2020) 3473, https://doi.org/10.3390/s20123473.

[12] L. Wang, A. Teleki, S.E. Pratsinis, P.I. Gouma, Ferroelectric WO3 nanoparticles for acetone selective detection, Chem. Mater. 20 (2008) 4794–4796, https://doi.org/10.1021/cm800761e.

[13] T.T. Tung, D. Losic, S.J. Park, J.F. Feller, T. Kim, Core-shell nanostructured hybrid composites for volatile organic compound detection, 10 Spec Iss, Int. J. Nanomed. (2015) 203–214, https://doi.org/10.2147/IJN.S88305.

[14] M. Šetka, F.A. Bahos, O. Chmela, D. Matatagui, I. Gràcia, J. Drbohlavová, S. Vallejos, Cadmium telluride/polypyrrole nanocomposite based Love wave sensors highly sensitive to acetone at room temperature, Sens. Actuators B. 321 (2020) 128573, https://doi.org/10.1016/j.snb.2020.128573.

[15] L. Ruangchuay, A. Sirivat, J. Schwank, Electrical conductivity response of polypyrrole to acetone vapor: effect of dopant anions and interaction mechanisms, Synth. Met. 140 (2004) 15–21, https://doi.org/10.1016/S0379-6779(02)01319-X.

[16] G. Balaji, S. Rathinavel, S. Vadivel, Design and fabrication of clad removed fiber optic based NiCo2O4 sensor for detection of ethanol and acetone gases, Optik 228 (2021) 166216, https://doi.org/10.1016/j.ijleo.2020.166216.

[17] J. Huang, T. Yang, Y. Kang, Y. Wang, S. Wang, Gas sensing performance of polyaniline/ZnO organic-inorganic hybrids for detecting VOCs at low temperature, J. Nat. Gas. Chem. 20 (2011) 515–519, https://doi.org/10.1016/S1003-9953(10)60230-7.

[18] M. Tomić, M. Šetka, L. Vojkůvka, S. Vallejos, VOCs sensing by metal oxides, conductive polymers, and carbon-based materials, Nanomaterials 11 (2021) 552, https://doi.org/10.3390/nano11020552.

[19] W. Muangrat, T. Chodjarusawad, R. Maolanon, S. Pratontep, S. Porntheeraphat, W. Wongwiriyapan, Poly(methyl methacrylate) and thiophene-coated single-walled carbon nanotubes for volatile organic compound discrimination, Jpn. J. Appl. Phys. 55 (2016), https://doi.org/10.7567/JJAP.55.02BD04.

[20] J.G. Ibanez, M.E. Rincón, S. Gutierrez-Granados, M. Chahma, O.A. Jaramillo-Quintero, B.A. Frontana-Uribe, Conducting polymers in the fields of energy, environmental remediation, and chemical–chiral sensors, Chem. Rev. 118 (2018) 4731–4816, https://doi.org/10.1021/acs.chemrev.7b00482.

[21] S. Bhattacharya, A.K. Agarwal, O. Prakash, S. Singh, Sensors for Automotive and Aerospace Applications, Springer, 2018.

[22] M. Yucel, O. Akin, M. Cayoren, I. Akduman, A. Palaniappan, B. Liedberg, G. Hizal, F. Inci, U.H. Yildiz, Hand-held volatilome analyzer based on elastically deformable nanofibers, Anal. Chem. 90 (2018) 5122–5129, https://doi.org/10.1021/acs.analchem.7b05187.

[23] M.H. Naveen, N.G. Gurudatt, Y.-B. Shim, Applications of conducting polymer composites to electrochemical sensors: a review, Appl. Mater. Today 9 (2017) 419–433, https://doi.org/10.1016/j.apmt.2017.09.001.

[24] T. Sen, S. Mishra, N.G. Shimpi, Synthesis and sensing applications of polyaniline nanocomposites: a review, RSC Adv. 6 (2016) 42196–42222, https://doi.org/10.1039/C6RA03049A.

[25] R. Rella, J. Spadavecchia, M.G. Manera, S. Capone, A. Taurino, M. Martino, A. P. Caricato, T. Tunno, Acetone and ethanol solid-state gas sensors based on TiO2 nanoparticles thin film deposited by matrix assisted pulsed laser evaporation, Sens. Actuators B. 127 (2007) 426–431, https://doi.org/10.1016/j.snb.2007.04.048.

[26] S.-J. Young, Y.-H. Liu, Z.-D. Lin, K. Ahmed, M.N.I. Shiblee, S. Romanuik, P. K. Sekhar, T. Thundat, L. Nagahara, S. Arya, R. Ahmed, H. Furukawa, A. Khosla, Multi-walled carbon nanotubes decorated with silver nanoparticles for room temperature gas sensing, J. Electrochem. Soc. 167 (2020) 167519, https://doi.org/10.1149/1945-7111/abd1be.

[27] H.D. Duong, Y. Shin, J.I. Rhee, Development of fluorescent pH sensors based on a sol-gel matrix for acidic and neutral pH ranges in a microtiter plate, Microchem. J. 147 (2019) 286–295, https://doi.org/10.1016/j.microc.2019.03.036.

[28] A. Tariq, J. Baydoun, C. Remy, R. Ghasemi, J.P. Lefevre, C. Mongin, A. Dauzères, I. Leray, Fluorescent molecular probe based optical fiber sensor dedicated to pH measurement of concrete, Sens. Actuators B. 327 (2021) 128906, https://doi.org/10.1016/j.snb.2020.128906.

[29] D. Wencel, T. Abel, C. McDonagh, Optical chemical pH sensors, Anal. Chem. 86 (2014) 15–29, https://doi.org/10.1021/ac4035168.

[30] M.T. Rahman, Z. Barikbin, A.Z.M. Badruddoza, P.S. Doyle, S.A. Khan, Monodisperse polymeric ionic liquid microgel beads with multiple chemically switchable functionalities, Langmuir 29 (2013) 9535–9543, https://doi.org/10.1021/la401613w.

[31] A.U. Alam, Y. Qin, S. Nambiar, J.T.W. Yeow, M.M.R. Howlader, N.-X. Hu, M. J. Deen, Polymers and organic materials-based pH sensors for healthcare applications, Prog. Mater. Sci. 96 (2018) 174–216, https://doi.org/10.1016/j.pmatsci.2018.03.008.

[32] K. Paek, H. Yang, J. Lee, J. Park, B.J. Kim, Efficient colorimetric pH sensor based on responsive polymer–quantum dot integrated graphene oxide, ACS Nano 8 (2014) 2848–2856, https://doi.org/10.1021/nn406657b.

[33] M.A. Sani, M. Tavassoli, H. Hamishehkar, D.J. McClements, Carbohydrate-based films containing pH-sensitive red barberry anthocyanins: application as biodegradable smart food packaging materials, Carbohydr. Polym. 255 (2021) 117488, https://doi.org/10.1016/j.carbpol.2020.117488.

[34] C. von Bültzingslöwen, A.K. McEvoy, C. McDonagh, B.D. MacCraith, I. Klimant, C. Krausec, O.S. Wolfbeis, Sol-gel based optical carbon dioxide sensor employing dual luminophore referencing for application in food packaging technology, Analyst 127 (2002) 1478–1483, https://doi.org/10.1039/b207438a.

[35] S. Suklabaidya, S. Chakraborty, S. Sarkar, R. Paul, H. Banik, A. Chakraborty, D. Bhattacharjee, S. Majumdar, S.A. Hussain, Polydiacetylene-N-1-hexadecyl imidazole mixed film and its application toward the sensing of volatile organic compounds, gasoline, and pollution level in car exhaust, J. Phys. Chem. C 125 (2021) 15976–15986, https://doi.org/10.1021/acs.jpcc.1c04338.

[36] S. Dolai, S. Bhunia, S. Beglaryan, S. Kolusheva, L. Zeiri, R. Jelinek, Colorimetric polydiacetylene–aerogel detector for volatile organic compounds (VOCs), ACS Appl. Mater. Interfaces 9 (2017) 2891–2898, https://doi.org/10.1021/acsami.6b14469.

[37] M.O. Kim, M.Q. Khan, A. Ullah, N.P. Duy, C. Zhu, J.-S. Lee, I.S. Kim, Development of VOCs gas sensor with high sensitivity using colorimetric polymer nanofiber: A unique sensing method, Mater. Res. Express. 6 https://doi.org/10.1088/2053-1591/ab42a5.

[38] R.I. Stoian, B.K. Lavine, A.T. Rosenberger, pH sensing using whispering gallery modes of a silica hollow bottle resonator, Talanta 194 (2019) 585–590, https://doi.org/10.1016/j.talanta.2018.10.077.

[39] L. Palanikumar, M.T. Jeena, K. Kim, J.Y. Oh, C. Kim, M.-H. Park, J.-H. Ryu, Spatiotemporally and sequentially controlled drug release from polymer gatekeeper–hollow silica nanoparticles, Sci. Rep. 7 (2017) 46540, https://doi.org/10.1038/srep46540.

[40] O. Korostynska, K. Arshak, E. Gill, A. Arshak, Review on state-of-the-art in polymer based pH sensors, Sensors 7 (2007) 3027–3042, https://doi.org/10.3390/s7123027.

[41] X.M. Shi, L.-P. Mei, N. Zhang, W.-W. Zhao, J.-J. Xu, H.-Y. Chen, A polymer dots-based photoelectrochemical pH sensor: simplicity, high sensitivity, and broad-range pH measurement, Anal. Chem. 90 (2018) 8300–8303, https://doi.org/10.1021/acs.analchem.8b02291.

[42] M.I. Khan, K. Mukherjee, R. Shoukat, H. Dong, A review on pH sensitive materials for sensors and detection methods, Microsyst. Technol. 23 (2017) 4391–4404, https://doi.org/10.1007/s00542-017-3495-5.

[43] H. Hah, J. Kim, B. Jeon, S. Koo, Y. Lee, Simple preparation of monodisperse hollow silica particles without using templates, Chem. Commun. (2003) 1712–1713, https://doi.org/10.1039/B301521A.

[44] M.S. Sha, M.R. Maurya, S. Shafath, J.-J. Cabibihan, A. Al-Ali, R.A. Malik, K. K. Sadasivuni, Breath analysis for the in vivo detection of diabetic ketoacidosis, ACS Omega 7 (2022) 4257–4266, https://doi.org/10.1021/acsomega.1c05948.

[45] Y.Y. Maruo, K. Tachibana, Y. Suzuki, K. Shinomi, Development of an analytical chip for detecting acetone using a reaction between acetone and 2,4-dinitrophe-nylhidrazine in a porous glass, Microchem. J. 141 (2018) 377–381, https://doi.org/10.1016/j.microc.2018.05.041.

[46] A., D. Worrall, J.A. Bernstein, A.P. Angelopoulos, Portable method of measuring gaseous acetone concentrations, Talanta 112 (2013) 26–30, https://doi.org/10.1016/j.talanta.2013.03.052.

Jea Jung Park is a research staff in a research institute of the Korea Initiative for Fostering University of Research and Innovation (KIURI). He received a Ph.D. degree from Yonsei University in 2020. His research focuses on using nanoparticles of various materials to detect trace amounts of gases in sensor and coating technologies.

Jihyun Lee received a Bachelor's degree in Material Science and Engineering at Kookmin University in 2020. Since 2020, she is currently a Ph.D. candidate at the Department of Materials Science and Engineering at Yonsei University under the supervision of Prof. Wooyoung Lee. She is currently studying on nanostructured metal-oxide semiconductor gas sensors.

Gye Hyeon Kim is a master's degree researcher in Yonsei University Industry Foundation. She earned a Master's degree in Chemical Engineering from Sungkyunkwan University in 2022. Her primary research focus lies in the practical development of conductive materials based on natural electronic materials and their applications in electronics. Her research endeavors have been dedicated to the development and real-world implementation of materials that can be utilized in electronics, such as sensors and electrodes.

Joonghyun Kim is professor of the Chemical and Biomolecular Engineering at Yonsei University in Korea. His research spans various domains, including the development of highly conducting polymers for transparent electrodes and thermoelectric devices, the synthesis and processing of nanoparticles and nanostructured functional materials, and the design and synthesis of nanostructured materials using supercritical fluids.

Hyun-Sook Lee received a Ph.D. degree in Physics at POSTECH in 2008. Since 2015, she has been working as a research professor in the Department of Materials Science and Engineering at Yonsei University. Her research interests are in various materials related to high-temperature superconductors, solid-state hydrogen storages, rare-earth/rare-earth-free permanent magnets, nanostructured metal oxide semiconductor gas sensors, and Pd-based hydrogen sensors.

Wooyoung Lee is the Underwood distinguished professor of the Department of Materials Science and Engineering at Yonsei University in Korea. He is also the Director of the Center for Super Critical Material Industrial Technology, National Core Materials Research Center and the institute of Korea Initiative for Fostering University of Research and Innovation. He is the President of The Korean Magnetics Society and a regular member of the National Academy of Engineering of Korea. In recent years, his research interests have centered on hydrogen sensors, various metal oxide semiconducting gas sensors, and breath analyzers. He is also studying rare-earth permanent magnets and thermoelectric materials and devices. He has received a number of awards in nano-related research areas including a Prime Minister Award (2023) in Nano Korea 2023, SeAH-Haiam Fellowship Award (2018) in The Korean Institute of Metals and Materials and a Service Merit Medal (2008) from the Government of Korea due to his contribution to the development of intellectual properties. He has authored and co-authored over 280 publications and has edited three special books on nanostructured materials and devices.